J|A|C|S
ARTICLES
Published on Web 00/00/0000

The Microenvironment Effect on the Generation of Reactive Oxygen Species by Pd−Bacteriopheophorbide

Yahel Vakrat-Haglili,[†] Lev Weiner,[§] Vlad Brumfeld,[†] Alexander Brandis,[†] Yoram Salomon,[‡] Brian McIlroy,[||] Brian C. Wilson,[||] Anna Pawlak,[⊥] Malgorzata Rozanowska,[⊥] Tadeusz Sarna,[⊥] and Avigdor Scherz*,[†]

Contribution from the Department of Plant Sciences, Weizmann Institute of Science, Rehovot, Israel, Department of Biological Regulation, Weizmann Institute of Science, Rehovot, Israel, Department of Chemical Services, Weizmann Institute of Science, Rehovot, Israel, Ontario Cancer Institute, Princess Margaret Hospital, Toronto, Canada, and Faculty of Biotechnology, Jagiellonian University, Krakow, Poland

Received June 27, 2004; E-mail: avigdor.scherz@weizmann.ac.il

Abstract: Generation of reactive oxygen species (ROS) is the hallmark of important biological processes and photodynamic therapy (PDT), where ROS production results from in situ illumination of certain dyes. Here we test the hypothesis that the yield, fate, and efficacy of the species evolved highly depend on the dye's environment. We show that Pd−bacteriopheophorbide (Pd−Bpheid), a useful reagent for vascular targeted PDT (VTP) of solid tumors, which has recently entered into phase II clinical trials under the code name WST09 (trade name TOOKAD), forms appreciable amounts of hydroxyl radicals, superoxide radicals, and probably hydrogen peroxide in aqueous medium but not in organic solvents where singlet oxygen almost exclusively forms. Evidence is provided by pico- and nanosecond time-resolved spectroscopies, ESR spectroscopy with spin-traps, time-resolved singlet oxygen phosphorescence, and chemical product analysis. The quantum yield for singlet oxygen formation falls from ∼1 in organic solvents to ∼0.5 in membrane-like systems (micelles or liposomes), where superoxide and hydroxyl radicals form at a minimal quantum yield of 0.1%. Analysis of photochemical products suggests that the formation of oxygen radicals involves both electron and proton transfer from ^{3}Pd−Bpheid at the membrane/water interface to a colliding oxygen molecule, consequently forming superoxide, then hydrogen peroxide, and finally hydroxyl radicals, with no need for metal catalysis. The ability of bacteriochlorophyll (Bchl) derivatives to form such radicals upon excitation at the near infrared (NIR) domain opens new avenues in PDT and research of redox regulation in animals and plants.

Introduction

Photodynamic therapy (PDT) is a relatively new treatment modality that relies on tissue intoxication by in situ reactive oxygen species (ROS) generated upon the coincidence of light, oxygen, and sensitizing molecules. Since each reactant is nontoxic and the produced ROS are highly toxic but have very short lifetimes, the toxic effect is temporarily and spatially limited, providing more selective therapy than currently applied chemo or radiotherapies.

It is generally believed that in processes mediated by the first and second generation of photosensitizers, the primary biological effect of PDT is caused by singlet oxygen molecules formed through a "Type II mechanism"[1] in tumor and endothelial cells of the tumor tissue. This "working hypothesis" is frequently supported by in vitro experiments where the photochemistry and photophysics of different sensitizers are studied in hydrophobic media, thus attempting to mimic the in situ cellular environment. However, the actual environment where the primary photodynamic action takes place may be quite heterogeneous and, therefore, greatly influence the type, lifetime, and reactivity of the generated ROS. For example, superoxide anions have very low solubility in membranes, but become soluble in aqueous solutions or upon protonation. The hydroperoxyl radical is not only more soluble and mobile in phospholipid membranes, compared with the superoxide anion radical, but also markedly more reactive.[2,3] A small number of hydroxyl radicals may initiate a chain reaction of phospholipid peroxidation that is significantly more toxic to the tumor tissue than peroxidation by a much higher concentration of singlet oxygen molecules.

The environment of the photodynamic (PD) events becomes a critical issue when it concerns the therapeutic benefits of cell-specific drug delivery. A favorable approach to this issue is the conjugation of the sensitizers to cell homing molecules, which results in targeting of the sensitizing molecules to specific receptors on the cell membrane.[4−8] Here, the PD effect may be

[†] Department of Plant Sciences, Weizmann Institute of Science.
[‡] Department of Biological Regulation, Weizmann Institute of Science.
[§] Department of Chemical Services, Weizmann Institute of Science.
[||] Ontario Cancer Institute, Princess Margaret Hospital.
[⊥] Faculty of Biotechnology, Jagiellonian University.

(1) Foote, C. S. *Am. Chem. Soc. Symp. Ser.* **1987**, *1*, 22−38.
(2) De Grey, A. *DNA Cell Biol.* **2002**, *21*, 251−257.
(3) Muller, F. *J. Am. Aging Assoc.* **2000**, *23*, 227−253.
(4) Reddi, E. *J. Photochem. Photobiol., B* **1997**, *37*, 189−195.

Scheme 1

(a) Pd-Bpheid (TOOKAD) (b) Pd-2-Ac-Pheid (c) Pd-Porphyrin (Pd-Por)

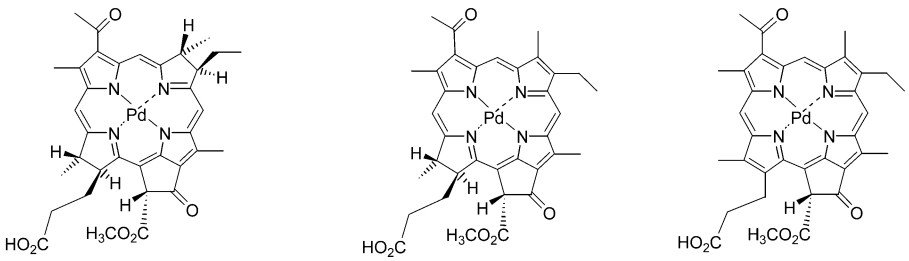

at the water/membrane interface. What ROS will be generated in such a case? Can we anticipate significant damage by the sensitizing molecules? It is quite likely that some amphiphilic sensitizers generate ROS in the aqueous interface of cellular membranes, whereas others act after endocytosis in different cell domains, such as lysosomes, mitochondrial membranes, nuclei, and so forth.[9−13] The environmental effect on ROS generation is also critical when considering the efficacy of vascular-targeted PDT (VTP) reagents that interact directly with oxygen in the plasma.[14] Notably, superoxide radicals generated under these conditions may play a key role in the vascular shut down, as discussed elsewhere.[14,15] Moreover, ROS generation in the vascular bed is accompanied by a sharp decrease in the concentration of oxygen. The oxygen depletion induces an additional oxidative stress on the tumor tissue.[14] To the best of our knowledge, there has been no systematic study of the environmental effect on ROS generation by any particular sensitizer, although this should be an important consideration when designing new sensitizers and modes of PDT applications.

Bacteriochlorophyll (Bchl) derivatives have been recognized for some time as good candidates for PDT sensitization. These molecules are characterized by a very high extinction coefficient for light absorption in the near infrared ($\lambda_{max} = 760-800$ nm, $\epsilon_{\text{diethyl ether}} \approx 10^5\ M^{-1}\ cm^{-1}$), where light penetrates deeply into the animal tissue. They have relatively low redox potentials[16] and a relatively high yield for inter system crossing (ISC) to the excited triplet state, which plays a key role in the formation of ROS. Unfortunately, native Bchl undergoes rapid photooxidation even under dim light conditions and demetalation in slightly acidic solutions. Therefore, native Bchl should not be used in pharmaceutical composition. Introduction of the heavy atom palladium to the molecule's central cavity was found to increase the stability of the Bchl macrocycle, the molecule's ISC rate constant, and the quantum yield for ROS formation.[17,18]

The Pd−Bpheid derivative (Scheme 1a) is a product of Pd-[Bchl] hydrolysis that can be synthesized by direct incorporation of Pd into bacteriophephorbide (Bpheid) and was found stable relative to BChl under dim light conditions.[19] Pd−Bpheid is hydrophobic and forms aggregates with a maximum absorption at ~820 and 900 nm in aqueous solutions. Yet, in micellar or liposomic solutions, and to some extent upon the addition of serum proteins, the pigments disaggregate into single molecules that absorb light at ~760 nm and are photochemicaly active. The phototoxicity of Pd−Bpheid, triggered by 760-nm illumination against endothelial cell-lines, is high compared with first- and even second- generation sensitizers ($LD_{50} \approx 5 \times 10^{-7}$ M under 10 J illumination).[19−21] The high extinction coefficient of this molecule ($\epsilon_{760\ nm} = 1 \times 10^5\ M^{-1}\ cm^{-1}$) enables sensitization in deep tissues. Pd−Bpheid was found highly phototoxic against tumor and endothelial cells in culture and to have a high curative effect on tumors implanted in animals.[14,21−28] A particular formulation of Pd−Bpheid has recently entered into phase II clinical trials under the code name WST09 (Steba-Biotech, France). The compound appeared nontoxic and efficacious in treating recurrent local prostate tumors in patients where radiation therapy failed.[29] The major target of Pd−Bpheid-PDT is the tumor vascular bed, which is also the primary site of ROS generation.[14,21,27] However, the mechanism underlying the compartmentalization of the sensitizer in the endothelial cells and different blood-borne particles during the very short drug/light interval (DLI) is not clear. It is likely that photosensitized oxidation at the cell membrane/lumen interface or even in the

(5) Rosenkranz, A. A.; Jans, D. A.; Sobolev, A. S. *Immunol. Cell Biol.* **2000**, *78*, 452−464.
(6) Rosenkranz, A. A.; Lunin, V. G.; Sergienko, O. V.; Gilyazova, D. G.; Voronina, O. L.; Jans, D. E.; Kofner, A. A.; Shumiantseva, M. A.; Mironov, A. F.; Sobolev, A. S. *Russ. J. Genet.* **2003**, *39*, 198−206.
(7) Akhlynina, T. V.; Jans, D. A.; Rosenkranz, A. A.; Statsyuk, N. V.; Balashova, I. Y.; Toth, G.; Pavo, I.; Rubin, A. B.; Sobolev, A. S. *J. Biol. Chem.* **1997**, *272*, 20328−20331.
(8) Gross, S.; Brandis, A.; Chen, L.; Rosenbach-Belkin, V.; Roehrs, S.; Scherz, A.; Salomon, Y. *Photochem. Photobiol.* **1997**, *66*, 872−878.
(9) Kessel, D.; Woodburn, K.; Gomer, C. J.; Jagerovic, N.; Smith, K. M. *J. Photochem. Photobiol., B* **1995**, *28*, 13−18.
(10) Kessel, D.; Woodburn, K.; Henderson, B. W.; Chang, C. K. *Photochem. Photobiol.* **1995**, *62*, 875−881.
(11) Kessel, D. *Photochem. Photobiol. Sci.* **2002**, *1*, 837−840.
(12) Kessel, D. *Photochem. Photobiol.* **1997**, *65*, 387−388.
(13) Kessel, D.; Poretz, R. D. *Photochem. Photobiol.* **2000**, *71*, 94−96.
(14) Gross, S.; Gilead, A.; Scherz, A.; Neeman, M.; Salomon, Y. *Nat. Med.* **2003**, *9*, 1327−1331.
(15) Mazor, O.; Kostenich, G.; Brandis, A.; Orenstein, A.; Salmon, Y.; Scherz, A. 9th International Photodynamic Association, May 20−23, Miyazaki, Japan, 2003.
(16) Noy, D.; Fiedor, L.; Hartwich, G.; Scheer, H.; Scherz, A. *J. Am. Chem. Soc.* **1998**, *120*, 3684−3693.
(17) Musewald, C.; Hartwich, G.; Pollinger-Dammer, F.; Lossau, H.; Scheer, H.; Michel-Beyerle, M. E. *J. Phys. Chem. B* **1998**, *102*, 8336−8342.
(18) Scherz, A.; Salomon, Y.; Scheer, H.; Hartwich, G.; Brandis, A. Patent No. WO 97/19081, PCT, 1997.
(19) Scherz, A.; Salomon, Y.; Brandis, A.; Scheer, H. U.S. Patent 6,569,846, 2003.
(20) Scherz, A.; Salomon, Y.; Fiedor, L. U.S. Patent No. 5,650,292, 1997.
(21) Schreiber, S.; Gross, S.; Brandis, A.; Hermelin, A.; Rosenbach-Belkin, V.; Scherz, A.; Salmon, Y. *Int. J. Cancer* **2002**, *99*, 279−285.
(22) Preise, D.; Mazor, O.; Koudinova, N.; Liscovitch, M.; Scherz, A.; Salomon, Y. *Neoplasia* **2003**, *5*, 475−480.
(23) Tremblay, A.; Leroy, S.; Freitag, L.; Copin, M. C.; Brun, P. H.; Marquette, C. H. *Photochem. Photobiol.* **2003**, *78*, 124−130.
(24) Borle, F.; Radu, A.; Fontolliet, C.; van den Bergh, H.; Monnier, P.; Wagnieres, G. *Br. J. Cancer* **2003**, *89*, 2320−2326.
(25) Borle, F.; Radu, A.; Monnier, P.; van den Bergh, H.; Wagnieres, G. *Photochem. Photobiol.* **2003**, *78*, 377−383.
(26) Bourre, L.; Thibaut, S.; Briffaud, A.; Rousset, N.; Eleouet, S.; Lajat, Y.; Patrice, T. *J. Photochem. Photobiol., B* **2002**, *67*, 23−31.
(27) Koudinova, N.; Pinthus, J. H.; Brandis, A.; Brenner, O.; Bendel, P.; Ramon, J.; Eshhar, Z.; Scherz, A.; Salomon, Y. *Int. J. Cancer* **2003**, *104*, 782−789.
(28) Chen, Q.; Huang, Z.; Luck, D.; Beckers, J.; Brun, P. H.; Wilson, B. C.; Scherz, A.; Salomon, Y.; Hetzel, F. W. *Photochem Photobiol.* **2002**, *76*, 438−445.
(29) Elhilali, M. In *Symposium-Steba-Biotech, the XVIII Congress of European Association of Urology*; Madrid, Spain; 2003.

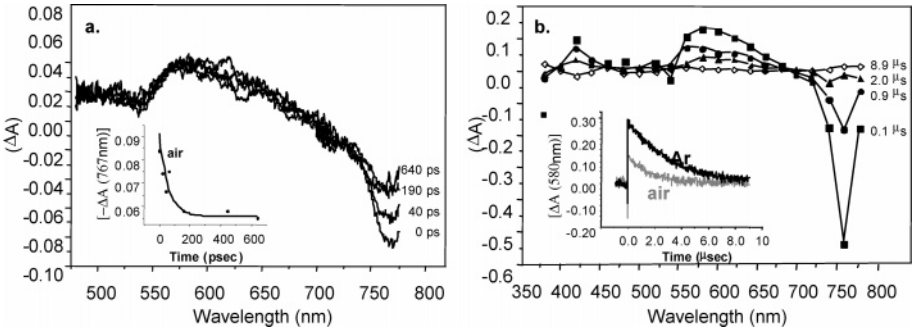

Figure 1. Time-resolved difference absorption spectra (ΔA) after flash photolysis of Pd−Bpheid in EggPC liposomes in: (a) the picosecond range, (b) the microsecond range. (Inserts) Decay of ΔA at 767 and 580 nm, respectively.

plasma is as important as the photodynamic action within the endothelial cells under these conditions. Therefore, resolving the effect of aqueous/micellar vs organic solutions upon ROS generation by Pd−Bpheid is important both for understanding the mechanism of its in vivo activity as well as for designing endothelial homing derivatives of this compound.

In studying the environmental effect on ROS generation by Pd−Bpheid, we have assumed that it pertains to both the photophysics and photochemistry of the sensitizer. Hence, we first studied the photophysical processes induced by illumination of Pd−Bpheid in micelles, liposomes, and organic solvents using time-resolved optical absorption spectroscopy in the pico-microsecond time domain, and measured the evolved singlet and triplet excited states. Next, we identified the type of ROS generated upon the photochemical processes in different microenvironments by using complementary techniques such as time-resolved singlet oxygen phosphorescence, ESR-oximometry, ESR-spin trapping, and chemical product analysis.

Our results indicate that the sensitizer's environment strongly affects the type and yield of the photogenerated ROS. In acetone, representing moderately polar organic solvents, photosensitized oxidation occurs predominantly via singlet oxygen, whereas superoxide and hydroxyl radicals may significantly contribute to the primary PD effect in an aqueous or mixed environment represented by micellar or lyposomal solutions. Furthermore, formation of these radicals by excited Pd−Bpheid is independent of the presence of transition metals and relies on concurrent electron and proton transfer from the triplet Pd−Bpheid to the ground state (triplet) dioxygen molecule. We believe that such environmental effects may also be relevant for other sensitizers and should be considered when designing new sensitizers for PDT such as those targeted to particular tissue/cell compartments.

Results

Observation of the Singlet and Triplet States of Excited Pd−Bpheid by Time-Resolved Absorption Spectroscopy. The photophysics of excited Pd−Bpheid was monitored in different microenvironments by measuring the absorption spectra before and after excitation at 770 and 532 nm with 14-ps (Figure 1a) and 5-ns pulses (Figure 1b). The spectra were characterized by four main features: (i) intensive bleaching at 760 nm, (ii) an absorption increase at 575 nm, (iii) an absorption decrease at 540 nm, and (iv) an absorption increase at 420 nm. Similar difference spectra appeared after excitation of the pigment in PBS solutions containing TX-100 instead of eggPC liposomes or in organic solutions (e.g., acetonitrile (AN) and acetone).

Table 1. Decay Rate Constants for the Singlet and Triplet States of Pd−Bpheid in Various Environments under Air-Saturated Conditions (k_{app} [s^{-1}]) and after Extensive Argon Purging (k_r[s^{-1}])

state	solvent	air-saturated solutions k_{app} [s^{-1}]	air-depleted solutions k_r [s^{-1}][a]
^{1}Pd−Bpheid	egg liposomes (767 nm)	1.7×10^{10}	1.7×10^{10}
	acetone	1.1×10^{10}	−
	micelles TX-100/PBS	1.2×10^{10}	−
^{3}Pd−Bpheid	egg liposomes	6.5×10^5	3.3×10^5
	acetone	5.9×10^6	2.0×10^5
	micelles TX-100/D_2O	7.4×10^5	2.9×10^5

[a] Measurements in TX-100 in the picosecond range were highly noisy because of extensive bubbles forming during air depletion, although rate constants similar to those observed in egg-liposomes were derived.

Both the bleaching at 760 nm and the absorption at 500−600 nm decayed in a biexponential fashion to the ground-state spectrum, with two time constants: a fast component with a 60−90-ps lifetime and a slower component with a microsecond lifetime.

The decay rate constant (1.7×10^{10} s^{-1}) of the fast component was found to be independent of the presence of molecular oxygen (Table 1) and close to the value measured for Pd−Bchl's first excited singlet state in toluene.[17] The fast component contributes approximately 40% of the apparent bleaching at 760−770 nm, and probably reflects fluorescence or stimulated emission from the excited singlet state. The long component of the 760-nm bleaching corresponds to the difference between the ground and excited states absorption. Since the latter is fairly small (D. Leopold, The Max-Born Institute, Berlin, personal communication), the absorption decrease at 760 nm at times >600 ps mostly reflected bleaching of the ground state. The absorption increase at 550−650 nm changed only slightly during the first hundreds of picoseconds, with a small decrease at 620−640 nm, but the signal-to-noise ratio was too low to allow refinement of the bleached signal.

Figure 1b shows the time-resolved absorption spectra obtained in the microsecond time domain (0.1−8.9 μs). The temporal absorption at 580 nm decayed with rate constants of 2.9×10^5 and 7.4×10^5 s^{-1} under anaerobic and aerobic conditions, respectively, in TX-100/PBS solutions. Similar values (6.5×10^5 and 3.3×10^5 sec^{-1}) were obtained in a suspension of EggPC liposomes. The decay rate constant in air-saturated acetone (5.9×10^5 s^{-1}) or AN (data not shown) was considerably higher (Table 1).

The oxygen-dependent lifetime prompted us to attribute the transient absorption at 500−600 nm to the triplet state of Pd−Bpheid. In agreement with this assignment, upon adding β-carotene (data not shown), the transient absorption of the

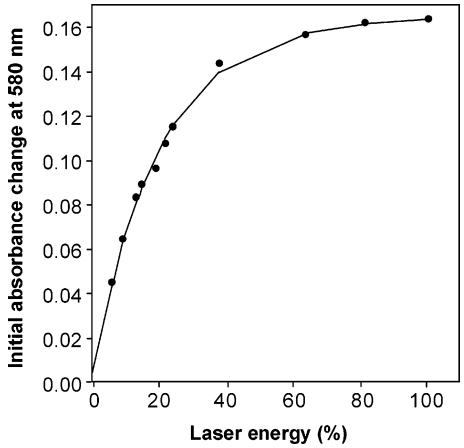

Figure 2. Initial absorbance changes of Pd−Bpheid in acetonitrile at 580 nm, induced by laser excitation as a function of laser energy. The sample was de-aerated by saturating with argon.

excited Pd−Bpheid at 580 nm decreased concurrently with an increase of the β-carotene excited triplet state absorption at 530 nm.[30] The decay rate constant of the Pd−Bpheid transient absorption increased linearly with increasing concentrations of the β-carotene, confirming the triplet identity of the transient absorption and suggesting an energy transfer rate of about 1.7 $\times$ 10^9 M^{-1} s^{-1}, at a yield of 37%.

The Quantum Yield (Φ_{ISC}) for Intersystem Crossing from the Singlet to the Triplet Excited State of Pd−Bpheid. Using the partial-saturation methods,[31−38] we derived the quantum yield for intersystem crossing (ISC) of Pd−Bpheid from the excited singlet to the excited triplet state. Figure 2 shows the dependence of the Pd−Bpheid's transient absorption at 580 nm on the energy of the exciting pulse.

The photophysical processes that Pd−Bpheid undergoes upon excitation can be described by the following set of equations:

$$^1\text{Pd-Bpheid}_0 \overset{\text{hv(763nm)}}{\Rightarrow} {}^1\text{Pd-Bpheid}_1 \quad (1)$$

$$^1\text{Pd-Bpheid}_1 \overset{k_{ic},k_f}{\Rightarrow} {}^1\text{Pd-Bpheid}_0 \quad (2)$$

$$^1\text{Pd-Bpheid}_1 \overset{k_{isc}}{\Rightarrow} {}^3\text{Pd-Bpheid}_1 \quad (3)$$

$$^3\text{Pd-Bpheid}_1 + {}^3\text{O}_2 \overset{k_c}{\Leftrightarrow} [{}^3\text{Pd-Bpheid}\ldots{}^3\text{O}_2] \overset{k_{ent}}{\Rightarrow} {}^1\text{Pd-Bpheid}_0 + {}^1\text{O}_2 \quad (4)$$

$$^3\text{Pd-Bpheid}_1 \overset{k_r=k_{ic}+k_{phos}}{\Rightarrow} {}^1\text{Pd-Bpheid}_0 + \text{hv (1170nm)} \quad (5)$$

where k_{ic}, k_f ,and k_{isc} are the rate constants of the Pd−Bpheid decay from its first excited singlet state to the ground state by radiationless transition, fluorescence, and *ISC* (to the excited triplet), respectively. The symbols k_c, k_{ent}, and k_{phos} are the rate constants for the collision complex formation between Pd−Bpheid in its first excited triplet state and oxygen molecules, the energy transfer between the two, and phosphorescence from the excited Pd−Bpheid, respectively.

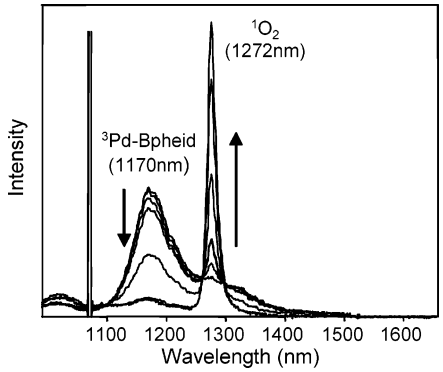

Figure 3. Phosphorescence spectrum of Pd−Bpheid in acetone at different times after starting nitrogen (99%) purging. OD_{535} (Pd−Bpheid) = 1. Excitation was performed with 1.5 mW, 532-nm pulses from a Nd:YAG laser.

The triplet quantum yield (Φ_{isc}) is given by

$$\Phi_{isc} = \frac{k_{isc}}{(k_{isc} + k_f + k_{ic})} = \frac{k_{isc}}{k_S} \quad (6)$$

Following Carmichael and Hug,[36−38] after laser excitation, the change in absorbance at the wavelength of analysis can be written as

$$(\Delta A) = (\epsilon_T - \epsilon_0)[S_0](l - \exp(-(2303\epsilon_0^{ex}E_p(t))\Phi_{isc}t)l \quad (7)$$

where ϵ_T and ϵ_0 are the molar extinction coefficients [M^{-1} cm^{-1}] of the triplet excited state and the singlet ground state, respectively, at the wavelength of analysis; ϵ_0^{ex} is the ground-state molar absorption coefficient (M^{-1} cm^{-1}) at the laser excitation wavelength; $E_p(t)$ is the photonic irradiance (Einstein s^{-1} cm^{-2}), and l is the optical path length [cm].

Experimentally, Φ_{isc} was derived by measuring the change in absorption (ΔA) at 580 nm, due to triplet state formation, as a function of E in AN saturated with argon (Figure 2). The experimental curve was then fitted by eq 7 with Φ_{isc} as the only free parameter. The value obtained for Φ_{isc} ($\geq$0.98) was close to 100%.

A similar value was found for Φ_{isc} in acetone by comparing the Pd−Bpheid phosphorescence in the two solvent systems in air-depleted solutions.

Emission Spectra from the Pd−Bpheid Triplet State and Energy Transfer to Molecular Oxygen. a. In Organic Solvents. Figure 3 illustrates the emission spectra of Pd−Bpheid recorded by FTIR in aerated and de-aerated acetone.

The emission at 1272 nm is indicative of singlet oxygen in solution,[39] whereas the small and broad signal centered at 1170 nm probably originates from the ^{3}Pd−Bpheid$_1$ emission. A similar signal (at 1168 nm) was previously assigned to ^{3}Pd−Bchl$_1$ phosphorescence.[40] Consistent with the assignment, nitrogen bubbling enhanced the intensity of the 1170-nm signal while reducing the emission at 1272 nm. Purging the solution with air reversed the observed signal intensities. The emission of ^{3}Pd−Bpheid$_1$ is broad and consists of a shoulder that extends to ~1370 nm. This signal may significantly contribute to the apparent 1272-nm emission at intermediate oxygen concentrations and below. The 1272-nm emission had to be corrected

(30) Nielsen, B. R.; Jorgensen, K.; Skibsted, L. H. *J. Photochem. Photobiol., A* **1998**, *112*, 127−133.
(31) Frimer, A. A., Ed. *Singlet Oxygen: Polymers and Biomolecules*; CRC Press: Boca Raton, 1985; Vol. IV.
(32) Bensasson, R.; Goldschmidt, C. R.; Land, E. J.; Truscott, T. G. *Photochem. Photobiol.* **1978**, *28*, 177.
(33) Lachish, U.; Infelta, P. P.; Gratzel, M. *Chem. Phys. Lett.* **1979**, *62*, 317−319.
(34) Masuhara, H.; Ohwada, S.; Mataga, N.; Itaya, A.; Okamoto, K.; Kusabayashi, S. *J. Phys. Chem.* **1980**, *84*, 2363−2368.
(35) Jacques, P.; Braun, A. M. *Helv. Chim. Acta* **1981**, *64*, 1800−1806.
(36) Hug, G. L.; Carmichael, I. *J. Photochem.* **1985**, *31*, 179−192.
(37) Carmichael, I.; Hug, G. L. *J. Phys. Chem.* **1985**, *89*, 4036−4039.
(38) Carmichael, I.; Hug, G. L. *J. Phys. Chem. Ref. Data* **1986**, *15*, 1−250.
(39) Parker, J. G.; Stanbro, W. D. *J. Photochem.* **1984**, *25*, 545−547.
(40) Hartwich, G.; Fiedor, L.; Simonin, I.; Cmiel, E.; Schafer, W.; Noy, D.; Scherz, A.; Scheer, H. *J. Am. Chem. Soc.* **1998**, *120*, 3675−3683.

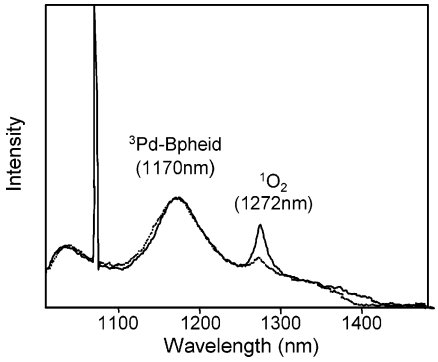

Figure 4. Phosphorescence spectra of Pd−Bpheid in 3% TX-100 with PBS (dotted line) or D_2O (solid line).

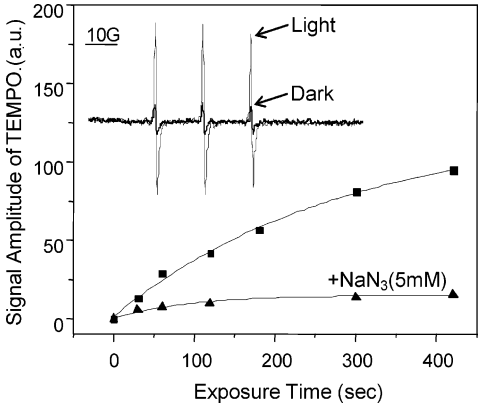

Figure 5. Evolution of the TEMPO• ESR signal intensity during illumination of a Pd−Bpheid and TEMP (0.13 M) in 1.5% TX-100/PBS in the absence (squares) and in the presence (triangles) of NaN_3 (5mM). (Insert) TEMPO• ESR signal; the temporal evolution of the first line was monitored.

for this contribution when used to measure the singlet oxygen concentration (see below).

The spectral changes that accompanied deoxygenation consisted of an isosbestic point at ∼1254 nm, suggesting conversion of one emitting form (singlet oxygen) to another (^{3}Pd−Bpheid$_1$), thus indicating that two emitting species are involved. Notably, singlet oxygen generation by Pd−Bheid was found ∼30% and ∼40% more efficient than by mTHPC and Photofrin R, respectively (measurements were performed in ethanol because of better solubilization compared with acetone, data not shown).

b. In Micelles (TX-1003%). The emission spectrum of Pd−Bpheid in a 3% TX-100 solution was markedly different from that recorded in acetone. In particular, excitation at 532 nm generated a major peak at 1170 nm and a minor one at 1272 nm in aerated solution. Although the emission at 1272 nm increased by a factor of 8 when the water was replaced by D_2O, and after subtracting the Pd−Bpheid emission in this wavelength, the estimated quantum yield for singlet oxygen generation in TX-100 /D_2O was about half of that observed in acetone (Figure 4).

Upon purging nitrogen to the Pd−Bpheid/TX-100 solution, the spectrum became similar to that recorded in de-aerated acetone; namely, the 1170-nm emission significantly increased whereas the 1270-nm peak vanished. This effect was reversed upon aeration. Interestingly, the 1170-nm emission intensity was almost identical in acetone and TX-100/water/D_2O for the same pigment concentration.

Generation of singlet oxygen was independently monitored by the ESR-spin trap technique. Figure 5 shows the ESR spectrum of TEMPO• generated upon illumination of Pd−Bpheid in TX-100 (778 nm, 13.2 mW cm^{-2}) in the presence of the spin trap TEMP. Although this experimental approach for detecting singlet oxygen is indirect and very nonspecific, it can be used as a convenient method for comparing the efficiency of singlet oxygen generation in systems that have been shown by other, more specific methods to generate singlet oxygen.

Single-exponential curves with rate constants of $k = 4 \times 10^{-3}$ s^{-1} and 6×10^{-3} s^{-1} could fit well the time dependence of the TEMPO• signal during illumination in the absence and presence of the singlet oxygen quencher NaN_3 (5 mM). The dramatic attenuation of the TEMPO• signal intensity but not its kinetics, in the presence of NaN_3, supports the notion that the ESR signal originates in singlet oxygen.

The formation of singlet oxygen during illumination of Pd−Bpheid in TX-100 micelles/D_2O, was further demonstrated by ESR oximetry.[41] Upon adding histidine during illumination, the oxygen concentration rapidly decreased. The addition of NaN_3 (10 mM) significantly slowed the oxygen consumption (Supporting Information, Figure 1).

The Quantum Yield of Singlet Oxygen Generation by Excited Pd−Bpheid. The quantum yield for singlet oxygen generation was determined relative to that for Rose Bengal (RB) by measuring the luminescence intensity at 1272 nm after Pd−Bpheid excitation at 532 nm (Figure 6). To avoid errors due to different quenching, we examined the lifetime of the singlet oxygen generated by the two sensitizers (Table 2).

The measured lifetimes of singlet oxygen in acetone were found to be 55 μs (Table 2). Similar values were found for $^1O_2$ generated by phenalenone.[42] This value is typical for organic solvents and more than 10 times longer than the lifetime of ^{3}Pd−Bpheid (Table 1). As showing in Table 2, in most studied samples there was no significant difference between the lifetime of singlet oxygen in the presence of Pd−Bpheid or RB, indicating that for both excited molecules, interaction with singlet oxygen does not constitute a significant means of decay. The last finding allowed derivation of the quantum yield for singlet oxygen generation by Pd−Bpheid ($\Phi_{Pd-Bpheid}$) relative to RB ($\Phi_{RB} = 0.75$[43,44]).

$$\Phi_{Pd-Bpheid} = \Phi_{RB}\frac{a_{Pd-Bpheid}}{a_{RB}} \qquad (8)$$

where $a_{Pd-Bpheid}$ and a_{RB} represent the slopes of the 1272-nm luminescence plotted against excitation laser intensity in the two environments (Figure 6).

This brings the quantum yield for singlet oxygen generation by ^{3}Pd−Bpheid in organic solutions to ∼100%.

The short lifetime of singlet oxygen in micelles ($\tau = 2.6$ μs, Table 2) was found to be similar to that of ^{3}Pd−Bpheid ($\tau =$ 3.0 μs). Under these conditions, the singlet oxygen concentration and lifetime could not be deduced from the 1272-nm emission. To overcome this difficulty, we replaced the water with D_2O. Here the long wavelength signal of singlet oxygen (36 μs) could

(41) Peng, Q.; Moan, J.; Nosland, J. M. *Ultrastruct. Pathol.* **1996**, *20*, 109−129.
(42) Shimizu, O.; Watanabe, J.; Imakubo, K.; Naito, S. *Chem. Lett.* **1999**, 67−68.
(43) Gandin, E.; Lion, Y.; Van de Vorst, A. *Photochem. Photobiol.* **1983**, *37*, 271−278.
(44) Murasecco-Suardi, P.; Gassmann, E.; Braun, A. M.; Oliveros, E. *Helev. Chim. Acta* **1987**, *70*, 1760−1773.

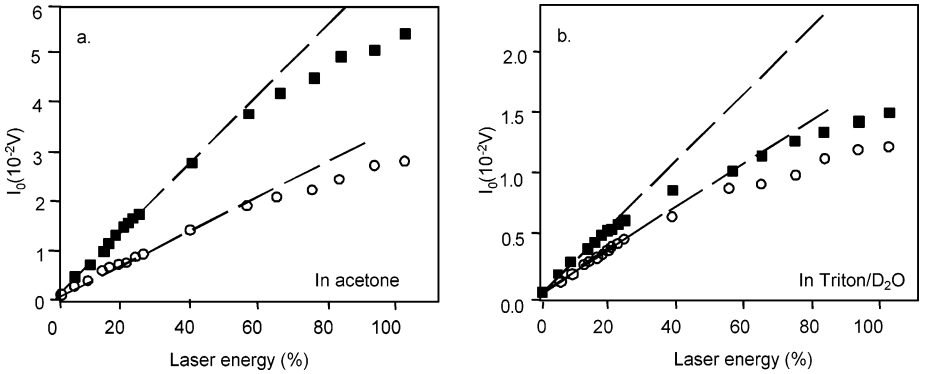

Figure 6. Intensity of the 1272-nm emission generated by excitation of Pd−Bpheid (squares) and Rose Bengal (circles) in: (a) acetone and (b) TX-100/D_2O, as a function of the laser energy.

Table 2. Lifetime of Singlet Oxygen ($^1O_2$) Generated by Pd−Bpheid($^1O_{2\ Pd-Bpheid}$) and Rose Bengal ($^1O_{2\ Rose\ Bengal}$) in Different Microenvironments

state	solvent	lifetime $\tau[\mu s]$
$^1O_{2\ Pd-Bpheid}$	acetone	55
	acetone/H_2O	8.2
	acetone/D_2O	37
	micelles TX-100/H_2O[a]	2.6
	micelles TX-100/D_2O	36
$^1O_{2\ Rose\ Bengal}$	acetone/H_2O	9.0
	acetone/D_2O	43
	micelles TX-100/H_2O	9.8
	micelles TX-100/D_2O	35

[a] The $^1O_2$ emission overlaps with the phosphorescence shoulder of ^{3}Pd−Bpheid at 1100−1370 nm. Hence, the lifetime measured at 1272 nm in aqueous solutions where the ^{3}Pd−Bpheid signal is very strong (Figure 4) probably reflects some average between the decay of ^{3}Pd−Bpheid (∼1.5 μs) and that of $^1O_2$. When the water is replaced by D_2O, the oxygen luminescence lifetime becomes significantly longer and only slightly perturbed by the sensitizer's phosphorescence. This problem does not exist for Rose Bengal since it has no phosphorescence that overlaps with that of oxygen.

be well-separated from the short-lasting signal of ^{3}Pd−Bpheid (3.4 μs) and was found to be similar to that generated by RB in TX-100/D_2O (36 μs, Table 2).

To calculate $\Phi_{Pd-Bpheid}$ in 3% TX-100/D_2O, we subtracted the contribution of Pd−Bpheid to the 1272-nm emission from the overall signal intensity before substituting in eq 8. This reduces the value of $a_{Pd-Bpheid}/a_{RB}$ in TX-100/D_2O to ∼0.7 and substituting 70% for $\Phi_{Pd-Bpheid}$ in water[44−49] provides $\Phi_{Pd-Bpheid} = 0.5$.

The Environmental Effect on ^{3}Pd−Bpheid Interaction with Molecular Oxygen. Molecular oxygen quenches ^{3}Pd−Bpheid by means of energy transfer (enabled in collision complexes that have a singlet spin multiplicity), electron transfer (enabled in collision complexes that have a triplet spin multiplicity), and radiationless transitions (in complexes that have quintet spin multiplicity).[50] The dependence of the ^{3}Pd−Bpheid decay on the oxygen concentration is described by a pseudo-first-order reaction:

$$-\frac{d(^3\text{Pd}-\text{Bpheid})}{dt} = k_{app}[^3\text{Pd}-\text{Bpheid}] \qquad (9a)$$

where

$$k_{app} = k_r + k_T^{O_2}[^3O_2] \qquad (9b)$$

and

$$k_T^{O_2} = (k_{elt} + k_{ent} + k_{phys}) \qquad (9c)$$

where k_{phys}, k_{elt}, and k_{ent}, represent rate constants for physical quenching, electron and energy transfer, respectively, from the excited sensitizer to molecular oxygen.

Alternatively:

$$k_T^{O_2} = k_c(\Phi_{elt} + \Phi_{ent} + \Phi_{phys}) \qquad (10)$$

where k_c represents the rate constant for a collision complex formation between the excited Pd−Bpheid and molecular oxygen. The symbols Φ_{elt},Φ_{ent},Φ_{phys} represent the quantum yields for transfer of energy and electron from ^{3}Pd−Bpheid and for its physical quenching, respectively. The concentration of oxygen in air-saturated acetone is 2 mM.[51,52] Substituting this number and the values of ∼1, 5.9 × 10^6 s^{-1}, and 2 × 10^5 s^{-1} for Φ_{ent}, k_{app}, and k_r (see Table 1), respectively, eqs 9b and 10 yield 2.85 × 10^9 M^{-1} s^{-1} for $k_T^{O_2}$, bringing k_c close to the diffusion-limited rate constant. As shown above, in micellar solutions, Φ_{ent} decreases to ∼0.5, and k_{app} and k_r become equal to 7.4 × 10^5 and 2.9 × 10^5 s^{-1}, respectively. Substituting these numbers in eq 9b yields 4.5 × 10^5 s^{-1} for $k_T^{O_2}[^3O_2]$, a value that is ∼10-fold smaller than that in acetone. To derive the value of $k_T^{O_2}$, we need an estimate of the oxygen concentration in the sensitizer's vicinity. This concentration may vary from 0.2 mM at the micelle/water interface[53] to ∼2 mM at the micelle's inner core, assuming that the inner core is as hydrophobic as acetone. Substituting the first number in eq 9b brings $k_T^{O_2}$ to a value of 2.2 × 10^9 M^{-1} s^{-1}, similar to the rate constant in acetone. However, in that case Φ_{elt} must increase to ∼0.5 or k_c would increase by a factor of 2 to comply with eq 10. Both are unlikely to happen. Thus, we propose that the oxygen concentration in

(45) Martinez, L. A.; Martinez, C. G.; Klopotek, B. B.; Lang, J.; Neuner, A.; Braun, A. M.; Oliveros, E. *Photochem. Photobiol., B* **2000**, *58*, 94−107.
(46) Neckers, D. C. J. *J. Photochem. Photobiol., A* **1989**, *47*, 1−29.
(47) Bilski, P.; Dabestani, R.; Chignell, C. F. *J. Phys. Chem.* **1991**, *95*, 5784−5791.
(48) Hoebeke, M.; Gandin, E.; Decuyper, A.; Van de Vorst, A. *J. Photochem.* **1986**, *35*, 245−250.
(49) Martinez, L. A.; Braun, A. M.; Oliveros, E. *J. Photochem. Photobiol., B* **1998**, *45*, 103−112.
(50) Dzhagarov, B. M.; Gurinovich, G. P.; Novichenkov, V. E.; Salokhiddinov, K. I.; Shul'ga, A. M.; Ganzha, V. A. *Sov. J. Chem. Phys.* **1990**, *6*, 2098−2119.
(51) Korinek, M.; Dedic, R.; Soboda, A.; Hala, J. *J. Fluoresc.* **2004**, *14*, 71−74.
(52) Parker, C. A. *Photoluminescence of Solutions*; Elsevier: New York, 1968.
(53) Halliwell, B.; Gutteridge, J. M. C. *Free Radicals in Biology and Medicine*, 3rd ed.; Oxford University Press: New York, 1999; p 4.

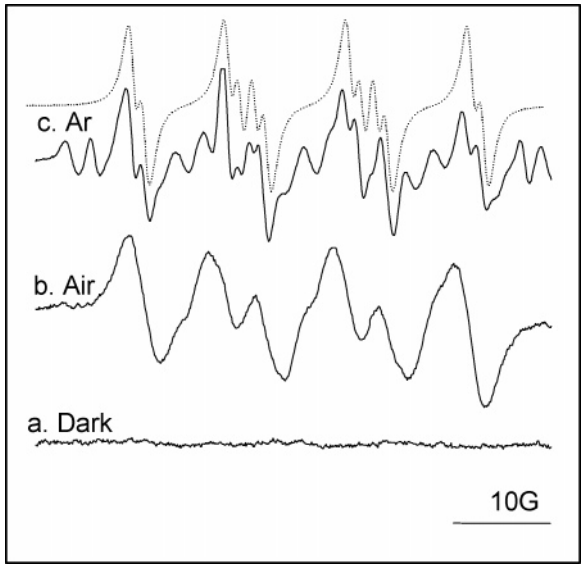

Figure 7. ESR spectrum of the DMPO−OOH adduct observed during illumination of Pd−Bpheid (25 μM) in acetone in the presence of DMPO (80 mM): (a) before illumination, (b) during illumination of an air saturated sample, and (c) during illumination of a partially de-aerated sample (solid line) and simulation (dotted line). Parameters used in the simulation were DMPO−OOH: $a_N = 12.5$ G, $a_{H\beta} = 8.0$ G, and $a_{H\gamma} = 1.6$ G.

the Pd−Bpheid vicinity is ~0.4 mM, twice as much as in water. This conclusion is supported by the following observations: (1) the calculated [$^3O_2$] concentration implies that the Pd−Bpheid approaches the membrane/water interface as previously suggested;[54] (2) taking 0.5 and 0.4 mM for Φ_{ent} and [$^3O_2$], respectively, reduces by 8−10-fold the yield of singlet oxygen generated by ^{3}Pd−Bpheid in micellar solutions relative to acetone, as experimentally observed by following the emission at 1272 nm and subtracting the contribution of the ^{3}Pd−Bpheid phosphorescence (Figures 4 and 6).

Evolution of $^{\bullet}$OH and $O_2^{-\bullet}$ Radicals during Excitation of Pd−Bpheid. a. In Acetone. Figure 7 illustrates the ESR spectrum that evolved upon illumination (at 778 nm, 13 mW) of Pd−Bpheid in aerated acetone in the presence of the spin trap DMPO.

The line shape and the hyperfine (hf) splitting of the main signal are typical of DMPO−OOH radicals generated by the reaction of DMPO and $O_2^{-\bullet}$ ($a_N = 12.5$ G, $a_{H\beta} = 8.0$ G, $a_H\gamma = 1.6$ G).[55] Partial replacement of the air by argon resulted in sharper lines and additional features on both the low- and high-field sides of the spectrum. The line narrowing attained at a lower oxygen concentration enabled the resolution of the hyperfine (hf) splitting and simulation of the line shape. The origin of the additional lines could not be resolved. Moreover, the $O_2^{-\bullet}$ yield could not be quantified because of the line broadening in air-saturated acetone and the absence of a reference signal such as that used for the generation of hydroxyl radicals (see below).

b. In TX-100/PBS. Figure 8 shows the ESR spectrum that evolved upon irradiation (13 mW, 778 nm) of Pd−Bpheid in micelles TX-100/chelexed PBS in the presence of 80 mM DMPO (insert). The generated quartet achieved maximum intensity within one hundred seconds of illumination, and its

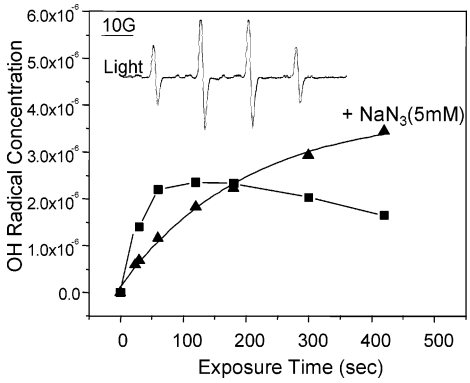

Figure 8. Evolution of the DMPO−OH adduct upon illumination of Pd−Bpheid in micelles TX-100/chelexed PBS in the presence (triangles) and absence (squares) of NaN_3 (5 mM). (Insert) Experimental (noisy line) and simulated (smooth line) EPR spectra of the DMPO−OH adduct. Parameters used in the simulation were $a_N = 14.9$ G and $a_H = 14.6$ G.

hf splitting was typical of a DMPO−OH adduct ($a_N = 14.9$ G, $a_H = 14.6$ G).[55−57]

Similar spectra and kinetics were observed for Pd−Bpheid in PC liposomes (saturated or nonsaturated) (data not shown). Although the prompt generation of DMPO−OH proves that $^{\bullet}$OH radicals are formed under the experimental conditions, they could have been formed primarily during degradation of DMPO−$^1O_2$ adducts or DMPO−OOH adducts.[58] To check the first possibility, we monitored the evolution of the DMPO−OH signal in the presence of sodium azide (5 mM). The concentration applied was similar to that used for the TEMP/TEMPO$^{\bullet}$ system (Figure 5). As showing in Figure 8, at this concentration, NaN_3 slowed the formation of the DMPO−OH signal but markedly increased its intensity. Furthermore, in the absence or at very low NaN_3 concentrations, the prompt increase in the DMPO−OH signal intensity was quickly followed by a continuous decrease. This second component could not be observed at higher concentrations of NaN_3. The time dependence of the DMPO−OH adduct formation in the presence of 5 mM NaN_3 could be highly simulated by an exponential curve (with $k = 0.006$ s^{-1}), as described by the solid line in Figure 8. The rate constant for DMPO−OH evolution is about 2 times lower than that found for the TEMPO$^{\bullet}$ formation ($k = 4{\cdot}10^{-3}$s^{-1}). The marked difference between the two, in response to the addition of sodium azide, rules out the possibility that both originate from the same $^1O_2$ pool. In fact, Figure 8 shows that $^1O_2$ possibly interferes with the formation of the DMPO−OH signal. Still, the effect of NaN_3 on the initial rate of the evolution of DMPO−OH may suggest that singlet oxygen partially contributed to the formation of the hydroxyl radical adducts.

To provide further support for the formation of $^{\bullet}$OH radicals, we examined the generated EPR signal upon Pd−Bpheid illumination in the presence of the spin trap DEPMPO, a DMPO analogue. This spin trap forms stable adducts with both $O_2^{-\bullet}$/O_2H and $^{\bullet}$OH radicals,[59] and does not react with $^1O_2$. The obtained ESR signal (Figure 9, solid line) is typical of the

(54) Fisher, J. R. E.; Rosenbach-Belkin, V.; Scherz, A. *Biophys. J.* **1989**, *58*, 464−470.
(55) Buettner, G. R. *Free Radical Biol. Med.* **1987**, *3*, 259−303.
(56) Faraggi, M.; Carmichael, A.; Riez, P. *Int. J. Radiat. Biol.* **1984**, *46*, 703−713.
(57) Finkelstein, E.; Rosen, G.; Rauckman, E. *Arch. Biochem. Biophys.* **1980**, *200*, 1−16.
(58) Bilski, P.; Reszka, K.; Bilska, M.; Chignell, C. F. *J. Am. Chem. Soc.* **1996**, *118*, 1330−1338.
(59) Frejaville, C.; Karoui, H.; Tuccio, B.; Lemoigne, F.; Culcasi, M.; Pietri, S.; Lauricella, R.; Tordo, P. *J. Med. Chem.* **1995**, *38*, 258−265.

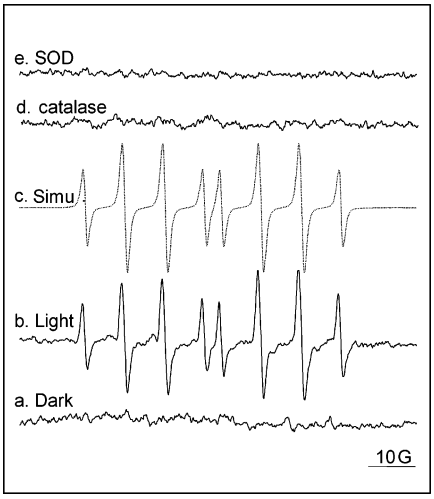

Figure 9. ESR spectrum of the adduct DEPMPO-OH obtained upon illumination of Pd−Bpheid (25 μM) in micelles TX-100/chelexed PBS in the presence of the spin trap DEPMPO (50 mM) (a) in the dark; (b) upon illumination; (c) computer simulation of *b* (a_N = 13.3 G, $a_{H\beta}$ = 12.5 G, $a_{H\gamma}$ = 0.2 G, a_P = 44.8 G) using NIEHS P.E.S.T. Winsim Simulation Software; (d) and (e) with the addition of catalase and SOD to the solution, respectively.

DEPMPO−OH radical and could be well simulated with a_N = 13.25 G, $a_{H\beta}$ = 12.53 G, $a_H\gamma$ = 0.17 G, and a_P = 44.75 G. The formation of this spin adduct was completely inhibited by catalase (a quencher of H_2O_2) and SOD (a scavenger of $O_2^{-\bullet}$) (Figure 9d,e), strongly suggesting that both $O_2^{-\bullet}$ and H_2O_2 are precursors of the $^\bullet$OH in the illuminated Pd−Bpheid system.

The concentration of $^\bullet$OH generated by photoexcited Pd−Bpheid in TX-100 micelles/PBS, as shown in Figure 8, was calculated from $S_{DMPO-OH}$, the intensity of the DMPO−OH ESR signal (after integration) relative to that of a standard, S_{stn} ([2,2,5,5 tetramethyl 3-pyrrolin-1-oxyl-3-carboxylic acid].

$$[^\bullet OH] = 3(S_{DMPO-OH}/S_{stn})\,[stn] = 2.2\ \mu M \qquad (11)$$

where the factor 3 compensates for the efficiency of DMPO to trap $^\bullet$OH.[60]

The number of $^\bullet$OH radicals generated in the entire experimental volume *V* is

$$N_{OH} = N_0[^\bullet OH]V = 7.6 \times 10^{14} \qquad (12)$$

where N_0 is the Avogadro number and V = 600 μL.

$^1N_{exc}$, the number of Pd−Bpheid molecules excited to the singlet state within 30 s, is given by

$$^1N_{exc} = [N_g]N_0\sigma_{760nm}f_{778nm}\cdot I_t l = 8.2 \times 10^{17} \qquad (13)$$

where N_g is the ground-state concentration of Pd−Bpheid (~26 μM), $\sigma_{760\ nm}$, the cross section for the optical absorption of Pd−Bpheid at 760 nm, is assumed to be similar to that of Pd−Bchl ($\sigma^{Pd-Bchl}{}_{760\ nm} = 1.2 \times 10^{-16}$cm^2, D. Leopold, Max-Born Institute, unpublished data). *f* is a correction factor corresponding to the differences in absorption wavelength (f = $OD_{778\ nm}/OD_{760\ nm}$ = 0.58), I_t is the number of photons supplied by the 778-nm diode laser during *t* seconds of illumination ($I_{t=30s} = 1.5 \times 10^{18}$), and *l* is the light pathway (0.5 cm).

(60) Carmichael, A. J.; Makino, K.; Riesz, P. *Radiat. Res.* **1984**, *100*, 222−234.

Under these experimental conditions, the number of excited Pd−Bpheid molecules in the triplet state is given by $^3N_{exc}$ = $^1N_{exc}\phi_{isc}$, which brings the apparent quantum yield for $^\bullet$OH generation in TX-100 to

$$\Phi_{\bullet OH} = \frac{N_{\bullet OH}}{^3N_{exc}} = \frac{7.6 \times 10^{14}}{[\Phi_{isc}](8.2 \times 10^{17})} = 0.1\% \qquad (14)$$

The findings disclosed thus far suggest that excitation of Pd−Bpheid in an oxygenated environment generates singlet oxygen, superoxide, hydrogen peroxide, and hydroxyl radicals in a medium-dependent fashion. The formation of these different ROS takes place under experimental conditions in which the metal ions have been removed (the solutions were treated by chelex resin and DTPA), and the only remaining reducing agent is the excited ^{3}Pd−Bpheid. Oxidation of Pd−Bpheid is expected to result in the formation of several photoproducts. Careful examination of the involved photochemistry provided additional information that was found useful in suggesting a scheme for the formation of the observed ROS.

Photochemical Degradation of Pd−Bpheid. a. In Acetone. The transient absorption of Pd−Bpheid in acetone after excitation by a single flash appeared to completely decay back into the ground-state absorption. However, subjecting Pd−Bpheid to continuous illumination (5 min) by the 778-nm diode laser (13 mW) in acetone resulted in ~25% bleaching of the 760-nm absorption and a concomitant small absorption increase, mainly at 660 and 430 nm (Supporting Information, Figure 2). No photochemical modification was observed in solutions that were thoroughly purged with argon.

b. In TX-100. About ~90% of the 760-nm transition of Pd−Bpheid was irreversibly lost when Pd−Bpheid was subjected to 778 nm (13 mW) illumination for 5 min in TX-100/PBS (Supporting Information Figure 3). The emerging spectral forms were resolved by MS and NMR after HPLC (A. Brandis, unpublished data). They appeared to represent the photochemical oxidation of Pd−Bpheid into three major products: (1) the Pd−Chlorin derivative: 2-desvynil-2-acetyl-Pd−pheophorbide (Pd-2-Ac−Pheid) (Scheme 1b), with maximum absorption at 660 (ϵ = 7.7 × 10^4 M^{-1} cm^{-1}), 423, and 395 nm, (2) Pd−porphyrin (Pd−Por) (Scheme 1c), with maximum absorption at 600 and 395 nm, and (3) an open-ring product with a major absorption at around 333 nm (Brandis et al., unpublished data). Figure 10 shows the absorption spectra of isolated Pd-2-Ac−Pheid (660 nm) and Pd−Por (660 nm) (insert Figure 10). Similar spectra were obtained by D. Brault et al. (Museum Natl. Hist. Nat. Paris, France, private communication)

The temporal concentrations of the 660-nm photochemical product (Pd-2-Ac−Pheid) and that of the Pd−Por (600 nm) were determined from their optical absorption at different times of illumination using their calculated extinction coefficients.

No photochemical modification of Pd−Bpheid was observed in either TX-100 or acetone when the samples were thoroughly purged with argon. Furthermore, the addition of reducing agents such as $Na_2S_2O_3$ (in excess) before illumination practically prevented irreversible changes in the spectral properties of Pd−Bpheid. These observations suggest that the 760-nm bleaching and the concurrent increase of the 660-, 600-, 430-, and 400-nm absorption bands are related to the oxidation of a ground or excited Pd−Bpheid by ground-state O_2 and/or ROS.

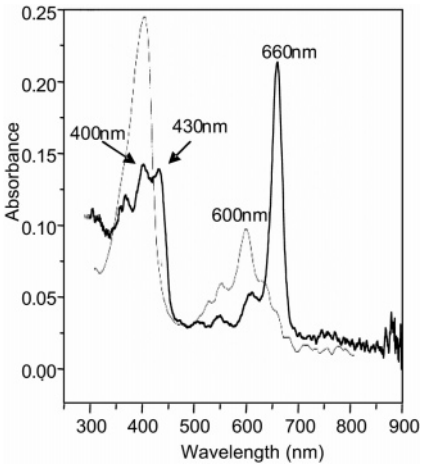

Figure 10. Absorption spectra of Pd−Chlorin derivative 2-desvynil, 2-acetyl-Pd−pheophorbide (Pd-2Ac−Pheid) in MeOH/chloroform with an absorption maximum at 660 nm (solid line) and Pd−porphyrin (Pd−Por) with a maximal absorption at 600 nm (dashed line).

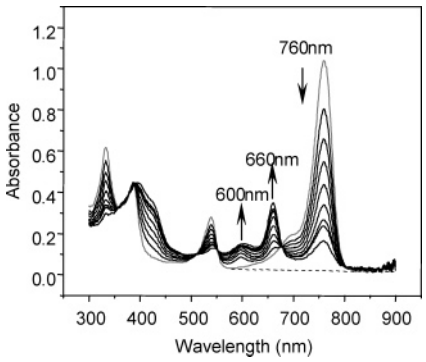

Figure 11. Photodegradation of Pd−Bpheid in 3% TX-100/chelexed PBS in the presence of 5 mM NaN_3. The optical absorption spectra show a bleaching of Pd−Bpheid (reduction of the 760- and 532-nm bands) and introduction of photoproducts with new bands at 660, 600, 423, and 395 nm.

To further characterize the oxidizing species involved, we performed the same experiment in the presence of NaN_3 (Figure 11). Under these conditions, the rate of Pd−Bpheid degradation slowed and the Pd-2-Ac−Pheid concentration increased, but its rate of formation also slowed. Additionally, there was a smaller and slower absorption increase corresponding to the formation of Pd−Por, suggesting that the addition of NaN_3 attenuated the photogeneration of Pd−Por but enhanced the formation or stabilized the Pd-2-Ac−Pheid molecules.

Replacing PBS with D_2O, where the lifetime of singlet oxygen is increased by 10 times (Table 2),[42,61−65] led to a ∼2-fold enhancement of the 760-nm bleaching (data not shown). No significant change was observed in the Pd-2-Ac−Pheid concentration compared with the observed value in TX-100/PBS. These results suggest that singlet oxygen is involved in the bleaching of Pd−Bpheid and the formation of the porphyrin but not in the generation of a chlorin-type product (Pd-2-Ac−Pheid).

On the basis of these observations, we propose that the permanent bleaching of Pd−Bpheid at 760 nm reflects photo-oxidation of the molecule. The need for oxygen underscores its role in the oxidation process. The dependence of the 600-nm band intensity (proportional to the formed Pd−Por) on the singlet oxygen concentration (controlled by NaN_3) and lifetime (controlled by D_2O) suggests that:

$$\text{Pd−Bpheid}_0 \overset{^1O_2}{\Rightarrow} \text{Pd−Por (600 nm)} \qquad (15)$$

In contrast, the increased concentration of the Pd-2-Ac−Pheid in the presence of NaN_3, at concentrations that appear to completely quench singlet oxygen, rules out the possibility that it is formed via interaction of Pd−Bpheid with singlet oxygen. Thus, we propose that Pd-2-Ac−Pheid forms via oxidation of the excited Pd−Bpheid by ground-state oxygen:

$$^3\text{Pd−Bpheid}_1 \overset{^3O_2}{\Rightarrow} \text{Pd-2-Ac−Pheid (660 nm)} \qquad (16)$$

This finding, when combined with the observed formation of superoxide radicals, suggests the concomitant formation of Pd-2-Ac−Pheid and superoxide radicals, for which we propose the following chain of events:

$$^3\text{Pd−Bpheid}_1 + {}^3O_2 \Rightarrow \text{Pd−Bpheid}^{+\bullet} + O_2^{-\bullet} \qquad (17)$$

The Pd−Bpheid$^{+\bullet}$ cation radical undergoes deprotonation and further oxidation:

$$\text{Pd−Bpheid}^{+\bullet} + O_2^{-\bullet} \Rightarrow \text{Pd−Bpheid}^{\bullet} + O_2H^{\bullet} \qquad (18a)$$

We assume that within the micelle the hydroperoxyl is fairly stable, although it should undergo rapid deprotonation within the aqueous phase at the experimental pH.

$$O_2H^{\bullet} \rightleftarrows O_2^{-\bullet} + H^+ \qquad (18b)$$

The Pd−Bpheid$^{\bullet}$ is highly unstable in the presence of hydroperoxyl and should undergo further oxidation and deprotonation:

$$\text{Pd−Bpheid}^{\bullet} + O_2H^{\bullet} \Rightarrow H_2O_2 + \text{Pd-2-Ac−Pheid} \qquad (19)$$

Thus, oxidation of ^{3}Pd−Bpheid by molecular oxygen in micellar solutions is expected to result in the sequential transfer of two electrons and two protons, generating consequently hydrogen peroxide and Pd-2-Ac−Pheid:

$$^3\text{Pd−Bpheid}_1 + {}^3O_2 \Rightarrow \text{Pd-2-Ac−Pheid} + H_2O_2 \qquad (20)$$

The proposed formation of hydrogen peroxide following excitation of ^{3}Pd−Bpheid$_1$ corroborates the ubiquitous requirement for this chemical entity in the course of forming $^{\bullet}$OH radicals, as inferred from the total quenching of the DEPMPO−OH adduct in the presence of catalase (Figure 9d). Furthermore, in the absence of available metal atoms under the experimental conditions (chelex, DTPA) ^{3}Pd−Bpheid should also provide the electron required for the reduction of hydrogen peroxide. To verify this hypothesis, we examined the interaction of H_2O_2 (4 mM) with excited Pd−Bpheid (Figure 12).

Evidently, hydrogen peroxide had no significant effect on the stability of Pd−Bpheid in the dark (data not shown). However, under 778-nm illumination, the rate of Pd−Bpheid degradation and the rate of the Pd-2-Ac−Pheid formation was

(61) Hurst, J. R.; Schuster, G. B. *J. Am. Chem. Soc.* **1983**, *105*, 5756−5760.
(62) Rodgers, M. A. *J. Am. Chem. Soc.* **1983**, *105*, 6201−6205.
(63) Rodgers, M. A. J. *Photochem. Photobiol.* **1993**, *37*, 99−103.
(64) Schmidt, R. *Am. Chem. Soc.* **1989**, *111*, 6983−6987.
(65) De la Pena, D.; Marti, C.; Nonell, S.; Martinez, L. A.; Miranda, M. A. *Photochem. Photobiol.* **1997**, *65*, 828−832.

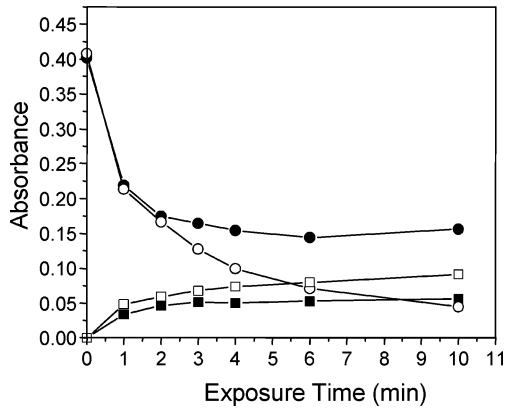

Figure 12. Kinetics of the photodegradation of Pd−Bpheid (760 nm) (circles) and Pd-2-Ac−Pheid (660 nm) (squares) upon illumination of Pd−Bpheid in 3% TX-100/chelexed PBS, in the absence (full shapes) and presence (open shapes) of H_2O_2 (4 mM).

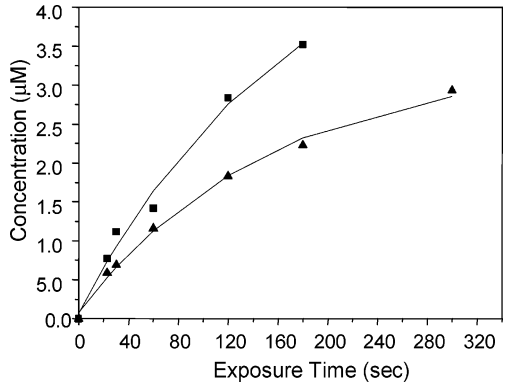

Figure 13. Formation kinetics of ·OH radicals (triangles) and the photoproduct Pd-2-Ac−Pheid (squares). The lines were constructed using exponential curve fitting with the formula $y = a + b(1 - \exp(-cx))$, where $a = 7.8e\text{-}6$, $b = 3.22e\text{-}6$, $c = 0.0066$, $r^2 = 0.997$ (for $y = [^{\bullet}OH]$) and $a = 7.24e\text{-}8$, $b = 5.35e\text{-}6$, $c = 0.0058$, $r^2 = 0.988$ (for $y =$ [Pd-2Ac−Pheid]).

significantly enhanced. Concomitantly, the intensity of the DMPO−OH signal was markedly increased in the presence of the added H_2O_2, thus suggesting that both excited Pd−Bpheid and hydrogen peroxide are needed for the formation of hydroxyl radicals.

$$^3\text{Pd−Bpheid}_1 + H_2O_2 \Rightarrow {}^{\bullet}OH + OH^- + H^+ + \text{Pd−Bpheid}^{\bullet} \quad (21)$$

$$\text{Pd−Bpheid}^{\bullet} + H_2O_2 \Rightarrow \text{Pd-2-Ac−Pheid} + {}^{\bullet}OH + OH^- + H^+ \quad (22)$$

Collectively, the photochemistry of excited Pd−Bpheid in the presence of oxygen in micellar solutions can be described by the following equation:

$$3^3\text{Pd−Bpheid}_1 + 2^3O_2 \Rightarrow 2{}^{\bullet}OH + 2OH^- + 2H^+ + 3\text{Pd-2-Ac−Pheid} \quad (23)$$

Thus, hydroxyl radicals are estimated to form at the same rate as the Pd-2-Ac−Pheid and at ∼0.7 times their yield, as experimentally observed (Figure 13).

The observed yield of hydroxyl radicals may be underestimated because of their possible interactions with ground-state Pd−Bpheid molecules and their degradation products. To confirm this possibility and to estimate the possible effect on the calculated yield, we subjected both Pd−Bpheid and Pd-2-Ac−Pheid (prepared according to Brandis et al.[19]) to ·OH radicals generated by the Fenton reaction in 3% TX-100 in the dark (Supporting Information, Figures 4−5). The rapid degradation of both the parent compound and its photochemical product (evident by the decrease of the 760- and 660-nm absorption, respectively) with no replacement byproducts that have substantial absorption in the vis−NIR domains indicates that Pd-2-Ac−Pheid is subjected to oxidative degradation by ·OH. Furthermore, the absence of the 600 nm product suggests that the interaction of ·OH with Pd-2-Ac−Pheid does not generate Pd−Por but instead probably generates an open-ring product(s) like other chlorophyllous pigments.[66,67]

Discussion

There is wide agreement that ROS play a key role in both constructive and destructive fundamental biological processes including pigmentation in photosynthesis, redox regulation, pathogen−host interactions, apoptosis, and development of nondifferentiated cells. Yet, defining chemically the oxygen form involved in this particular process in vivo is frequently difficult.[2] This deficiency reflects on both the lack of selective in vivo reporters and the lack of knowledge regarding the environmental effect on ROS evolution. Such knowledge is particularly important when designing sensitizers for PDT. The present study focuses on ROS generation by Pd−Bpheid, a novel VTP sensitizer that has recently entered into clinical trials.[29] Although we have shown that Bchl derivatives with Mg as the central metal are efficient sensitizers for ROS production[68,69] and VTP,[69,70] metal substitution with the heavy atom Pd has stabilized the compound and increased its phototoxicity by more than an order of magnitude both in vitro[19,21] and in vivo.[21,27] Current data indicate that ROS generation by Pd−Bpheid is limited to the tumor vasculature.[14,15] Vascular damage was also observed for hematoporphyrin derivatives (HPD) many years ago.[71,72] This may occur in the endothelial cell membrane at the interface with the aqueous lumen, within specific cellular compartments, or within the plasma. Importantly, the rapid depletion of oxygen observed during illumination of tumors after administration of Pd−Bpheid[14,70] probably indicates that the sensitizer interacts directly with plasma oxygen.

The heterogeneous vascular lumen milieu presents a variety of VTP targets susceptible to different types of ROS. For example, interactions of superoxide radicals with constitutive NO[73] should strongly interfere with anticoagulative processes. Hydroxyl radicals can initiate radical chain reactions with the endothelial cell membranes, which probably evolve into the

(66) Brown, S. B.; Smith, K. M.; Bisset, G. M.; Troxler, R. F. *J. Biol. Chem.* **1980**, *255*, 8063−8068.
(67) Curty, C.; Engel, N.; Iturraspe, J.; Gossauer, A. *Photochem. Photobiol.* **1995**, *61*, 552−556.
(68) Rosenbach-Belkin, V.; Chen, L.; Fiedor, L.; Tregub, I.; Pavlotsky, F.; Brumfeld, V.; Salmon, Y.; Scherz, A. *Photochem. Photobiol.* **1996**, *64*, 174−161.
(69) Zilberstein, J.; Schreiber, S.; Boloemers, M.; Bendel, P.; Neeman, M.; Schechtman, E.; Kohen, F.; Scherz, A.; Salomon, Y. *Photochem. Photobiol.* **2001**, *73*, 257−266.
(70) Kelleher, D. K.; Thews, O.; Scherz, A.; Salomon, Y.; Vaupel, P. *Br. J. Cancer* **2003**, *89*, 2333−2339.
(71) Star, W. M.; Marijnissen, H. P. A.; Vandenbergblok, A. E.; Versteeg, J. A. C.; Franken, K. A. P.; Reinhold: H. S. *Cancer Res.* **1986**, *46*, 2532−2540.
(72) Henderson, B. W.; Waldow, S. M.; Mang, T. S.; Potter, W. R.; Malone, P. B.; Dougherty, T. J. *Cancer Res.* **1985**, *45*, 572−576.
(73) Korbelik, M.; Parkins, C. S.; Shibuya, H.; Cecic, I.; Stratford, M. R. L.; Chaplin, D. J. *Br. J. Cancer* **2000**, *82*, 1835−1843.

second radical wave recently observed by Gross et al.[14] Hence, we explored how different microenvironments affect or even determine the nature and the quantum yield in the production of a particular ROS.

Considering photophysical processes, our data indicate, in agreement with the Russell−Sander rules for heavy atoms, that Pd substitution in Bchls results in a high quantum yield (~1) for photogeneration of the molecule's triplet state and an enhancement of its phosphorescence under anaerobic conditions. The measured high quantum yield for ISC is in agreement with the short lifetime of the excited singlet, reflected by the rapid depletion of the molecule's fluorescence ($k_f = 1.7 \times 10^{10}$ s^{-1}). In fact, within 200 ps after excitation, most of the lowest triplet excited state of Pd−Bpheid (>99%) is populated. This rapid process is probably due to the enhancement of spin−orbit coupling. Here we also show that the radiative lifetime of ^{3}Pd−Bpheid (τ_0) is short (~3 μs), even when compared with those of other Pd-substituted porphyrins.[74,75] Thus, we have concluded that efficient mechanisms exist in Pd−Bpheid for mixing the excited triplet with both the excited and ground singlet states. A similar high quantum yield for triplet state formation was previously observed for other Pd-containing porphyrins.[50] Remarkably, the half-lifetimes of these porphyrins' triplet states were longer by approximately 2 orders of magnitude compared with those reported here for Pd−Bpheid. Yet, the quantum yield for their ROS generation was considerably lower than the one reported here for the formation of singlet oxygen (close to 100% in air-saturated organic solvents). The rapid decay of ^{3}Pd−Bpheid to the ground state greatly limits the spatial range of phototoxicity, providing better contrast with nonilluminated domains.

Once the triplet state of the sensitizer is formed, the predominant reaction, in all studied systems, is energy transfer from ^{3}Pd−Bpheid to molecular oxygen to form singlet oxygen (eq 4). Nevertheless, a small but significant fraction of the excited dye molecules undergoes electron transfer. In organic solvents, ϕ_{ent} approaches unity and only a very small (but detectable) amount of superoxide radicals can be trapped. No hydroxyl radicals were observed. Although quantification of the superoxide radicals in acetone is difficult, some estimate is possible by: (1) following the DMPO−OOH signal intensity in acetone relative to that in micellar solutions and (2) following the oxidation of Pd−Bpheid upon the formation of superoxide radicals. As mentioned, we could observe no more than 25% bleaching of Pd−Bpheid after 5 min of illumination. In TX-100, both the quantum yield for energy transfer and the oxygen concentration decreased. Consequently, the concentration of singlet oxygen generated by the excited Pd−Bpheid decreased 10-fold compared with that with acetone solutions. At the same time, the signal intensity of the superoxide radicals was found to be higher than in acetone, and •OH radicals were formed at an apparent 0.1% yield. Furthermore, 90% of the Pd−Bpheid bleached. Taken together, the rate of radical formation appears to be higher than in acetone by an order of magnitude. Probably, in the relatively polar conditions presented at the micelle/water interface the charge-transfer character of the ^{3}Pd−Bpheid$_1$−^{3}O$_2$ collision complex is enhanced, thus increasing the electron-transfer yield.

The formation of hydroxyl radicals is thought to rely on the transfer of both electrons and protons from the Bpheid macrocycle to molecular oxygen in its ground state and, as such, may be independent of redox active metal ions (metal-catalyzed Fenton reaction). Although the quantum yield of the formation of the superoxide and hydroxyl radicals is collectively close to 0.2%, the extensive absorption and high ISC rate of the sensitizer lead to a substantial formation of radicals within a short illumination time (≥2 μM in 20 s of illumination). The formation of these radicals in vivo may markedly increase the efficacy of the sensitizer, particularly when the acidic environment of the tumor is considered.[2,3]

The stability and efficiency of Pd−Bpheid also make it a good model compound for studying radical generation by the excited macrocycle of chlorophylls (Chls) and Bchls, and the proposed photophysics and photochemistry may also apply to native Chls and Bchls. Although the triplet yield in these molecules is profoundly lower than in Pd−Bpheid, they may also form significant amounts of radicals when subjected to aqueous/micellar conditions.[76−78] Such radicals can significantly modify the local redox potentials and consequently be used as important triggers in the cellular response to light stress.

Acknowledgment. This research was supported in part by Steba-Biotech N.V. in collaboration with Negma-Lerads (France) and the Avron-Minerva Center for Photosynthesis. Singlet oxygen luminescence studies were supported by the National Center Institute of Canada (B.C.W.). A.S. is the incumbent of the Robert and Yadelle Sklar Professorial Chair for Biochemistry; Y.S. is the incumbent of The Tillie and Charles Lubin Professorial Chair in Biochemical Endocrinology. We are grateful to Dr. D. Leopold, the Max Born Institute, Berlin, for helpful discussions.

Supporting Information Available: Materials and methods: Materials (1), ESR Spectroscopy (2), ESR Oximetry (3), Time-Resolved Spectroscopy (4), Optical Absorption (5), Phosphorescence Spectra (6), Photochemical Degradation (7). Figure 1 shows the oxygen photouptake induced by irradiation of Pd−Bpheid in TX-100 micelles/D_2O. Figures 2,3 describe the absorption spectra of Pd−Bpheid in acetone under aerobic conditions and in TX-100. Figures 4,5 describe the absorption spectra of Pd−Bpheid and Pd-2-Ac−Pheid in the presence of •OH radicals formed by the Fenton reaction. This material is available free of charge via the Internet at http://pubs.acs.org.

JA046210J

(74) Brun, A. M.; Harriman, A. *J. Am. Chem. Soc.* **1994**, *116*, 10383−10393.
(75) Lo, L. W.; Koch, C. J.; Wilson, D. F. *Anal. Biochem.* **1996**, *236*, 153−160.
(76) Katz, S.; Vakrat, Y.; Brumfeld, V.; Weiner, L.; Gabelman, E.; Brandis, A.; Paul, A.; Hild, M.; Lendt, R.; Leopold, D.; Norris, J. R.; Salomon, Y.; Scherz, A. In *Proceedings of the 7th Biennial Congress*; Patrice, T., Ed.; International Photodynamic Association, ISPEN BIOTECH CD-Rom edition, 1998.
(77) Katz, S. Ph.D. Thesis. Weizmann Institute of Science, Rehovot, Israel, May, 1999.
(78) Scherz, A.; Salomon, Y.; Scheer, H.; Hartwich, G.; Brandis, A. U.S. Patent 6,333,319, 2001.